Novel Approximate Distribution of the Sum of Lognormal-Rician Turbulence Channels With Pointing Errors and Applications in MIMO FSO Links

Maoke Miao and Xiaofeng Li

***Abstract*—In this paper, an approximate closed-form probability density function expression for the sum of lognormal-Rician turbulence channels with Rayleigh pointing errors is developed. The results of Kolmogorov-Smirnov goodness-of-fit statistical tests show that the proposed approximation is highly accurate across a wide range of channel conditions. Also, the analysis of approximation error is presented in detail, and it indicates that a more efficient approximation can be achieved for larger coherence parameter r and smaller variance σ_z^2. To reveal the importance of proposed approximation, the closed-form expressions for the ergodic capacity, outage probability, and bit-error rate are derived in terms of Meijer's G-function. The performance of multiple-input multiple-output (MIMO) free-space optical (FSO) systems with equal gain combining (EGC) diversity technique are analyzed in detail under different scenarios, including the number of transmit and receive apertures, turbulence channels, and presence of pointing errors. It is observed that MIMO technology can offer a significant improvement in FSO performance when compared with the single-input single-output (SISO) systems. The ergodic capacity and BER performance at high signal-to-noise ratio are also obtained to provide further insights. Numerical results demonstrate the accuracy of the proposed approach.**

***Index Terms*—Lognormal-Rician turbulence channels, Rayleigh pointing errors, Kolmogorov-Smirnov statistical tests, MIMO FSO communication systems, equal gain combining (EGC) diversity.**

I. Introduction

FREE-space optical (FSO) communication, also known as outdoor optical wireless communication, has attracted considerable attention in recent years owing to its attractive bandwidth enhancement with unregulated spectrum. Furthermore, it can be anticipated that the FSO systems are likely to be noteworthy in the development of fifth-generation (5 G) and even perhaps 6 G as they efficiently overcome the important challenge caused by the radio frequency (RF) spectrum shortage [1], [2]. Despite these benefits of FSO technology, its widespread use has been hampered by its disappointing performance for long range links due to atmospheric turbulence-induced fading and pointing errors [3].

Plenty of statistical models have been proposed to characterize the turbulence-induced scintillation in FSO systems. The lognormal distribution is generally accepted for weak turbulence conditions [4], [5]. The Gamma-Gamma distribution is a double-stochastic scintillation model, and is shown to provide an excellent agreement with the experimental data in the moderate-to-strong turbulence regime [6]. However, it is noted that this model only performs well for receivers with small aperture [7]. Another important distribution is the lognormal-Rician distribution (also known as Beckmann), which comprises the lognormal, lognormal-Exponential and exponential distribution as its special cases [8]. The lognormal-Rician distribution not only agrees well with experimental data under weak-to-strong turbulence regime, but also is more accurate than the Gamma-Gamma distribution under a spherical wave assumption in particular [6], [9]. In recent years, a new universal turbulence model, named Málaga distribution has been widely advocated as it generalizes several turbulence-induced fading models (including Gamma-Gamma, lognormal) [10]. To apply these turbulence models to the analyses of practical FSO systems, we are often required to estimate the corresponding unknown parameters [11]. However, the PDF of Málaga distribution is expressed with a finite summation and includes plenty of parameters, and this makes it more difficult to estimate parameter when compared to Gamma-Gamma and lognormal-Rician channels. Also, it should be emphasized that the lognormal distribution is not an exact relation to the Málaga distribution, thus implying that lognormal-Rician is an approximate case of the Málaga distribution [12].

Apart from the turbulence-induced fading, the performance of FSO systems can be also severely deteriorated by the pointing errors due to building sway [13]. Various types of statistical models have been developed to describe the properties of pointing errors. The pioneer study of the pointing errors model in FSO systems can be found in [14], which considered the effects of beam width, detector size and independent identical Gaussian distributions for the elevation and the horizontal displacement.

Manuscript received May 14, 2022; revised May 30, 2022; accepted June 3, 2022. Date of publication June 8, 2022; date of current version June 17, 2022. This work was supported by the National Natural Science Foundation of China under Grant 61871347. *(Corresponding author: Xiaofeng Li.)*

Maoke Miao is with the School of Information and Electrical Engineering, Zhejiang University City College, Hangzhou 310015, China (e-mail: mmk1993@std.uestc.edu.cn).

Xiaofeng Li is with the School of Aeronautics and Astronautics, University of Electronic Science and Technology of China, Chengdu 611731, China (e-mail: lxf3203433@uestc.edu.cn).

Digital Object Identifier 10.1109/JPHOT.2022.3181041

Note that Rayleigh pointing errors model has been popularly used in a great deal of research articles in terms of its simplicity from a mathematical point of view as well as its realistic approach [15]–[17].

Multiple-input multiple-output (MIMO) technology has emerged as a promising technology to mitigate the effects of scintillation and pointing errors. Over the last couple of decades, a great amount of work has been conducted to study the performance of MIMO FSO links over different turbulence channels with pointing errors. For instance, the authors in [16]–[18] explored the ergodic capacity, bit-error rate (BER) and outage probability performance over Gamma-Gamma fading with pointing errors. The work in [19], [20] analyzed the BER, secrecy outage probability, and secrecy capacity performance of MIMO FSO links employing the maximal ratio combining (MRC) technique over the Málaga fading with pointing errors. With respect to the lognormal-Rician model, the results available so far for single-input single-output (SISO) and MIMO FSO systems in the literature are greatly limited since it does not have the closed-form PDF expression compared to the Gamma-Gamma and Málaga distribution. In [21], the authors investigated the BER performance of coherent FSO systems in lognormal-Rician turbulence employing the MRC and select combining (SC) via the Padé approximation method. Also, the authors in [22] employed the Gram-Charlier Series to study the BER performance of MIMO FSO systems with MRC. However, it must be noted that these two kinds of numerical methods provide limited information for performance analysis. Moreover, based on the moment-based method introduced in [23], asymptotic ergodic capacity at high signal-to-noise ratio (SNR) regime as well as at low SNR regime for SISO FSO links with Rayleigh pointing errors were developed in [24]. Nevertheless, this method can not be used to derive the ergodic capacity at medium SNRs. Recently, the authors in [25] derived the highly accurate expressions for the ergodic capacity and outage performance by using a series representation. However, they only considered the SISO cases and the BER performance was not evaluated.

Based on the aforementioned discussion, we investigate the performance of MIMO FSO systems over lognormal-Rician turbulence channels with pointing errors. The main contributions of this work are given as follows:

1) For the first time in the literature, the approximate analytic formula for the distribution of sum of Lognormal-Rician turbulence channels with pointing errors is developed by using a series representation. Then, the validity of the proposed approximation is investigated by employing the statistical tools, i.e., Kolmogorov-Smirnov (KS) goodness-of-fit tests. Also, the effects of channel model parameters on the approximation error are discussed in detail.
2) Based on the proposed approximation, we derive the ergodic capacity, outage probability, and BER performance for MIMO FSO systems using Equal gain combining (EGC) diversity technique over lognormal-Rician turbulence channels with pointing errors in closed-form. The ergodic capacity in the high SNR regime is obtained in terms of simple elementary functions and this enables us to analyze the effects of channel parameters and formulate the beam width optimization at the transmitter side. Also, the coding gain and diversity order are obtained from the asymptotic behavior of the derived BER performance via an asymptotic expansion of the Meijer's G-function. To the best of our knowledge, these results are new in the open literature.

The remainder of the paper is organized as follows. Section II presents the considered system and channel models. The closed-form expressions that approximate the PDF of the sum of lognormal-Rician turbulence channels with pointing errors variates are provided in Section III. Subsequently, the important performance metrics, namely, the ergodic capacity, the outage performance, and the BER performance for the MIMO FSO systems are obtained in Section IV. Finally, Section V presents some numerical simulation results to validate these analytical results, and the concluding remarks are given in Section VI.

II. System and Channel Model

A. System Model

Let us consider an intensity modulation and direct detection (IMDD)-based MIMO FSO systems with M_t transmitters and N_r receivers, where an OOK symbol $x \in \{0, 1\}$ is transmitted by all transmit apertures for each transmission time interval. Note that the IMDD systems are commonly used in the terrestrial FSO links due to their simplicity and low cost of implementation. Additionally, the transmitters or receivers are spatially separated by a sufficient distance that is lager than the coherence length ρ_0 in order to consider statistically independent and uncorrelated fading [26], [27]. Typically, they are placed with a few centimeters apart since ρ_0 is of the order of centimeters, as shown in [28], [29]. Moreover, a large amount of background radiation is collected by each receiver that offers a large field of view, and this justifies the use of the Gaussian noise model as a good approximation of the Poisson photon counting detection model [26]. Hence, the received signal at the jth, $j = 1, 2, \ldots, N_r$ receive aperture is given as

$$r_j = \eta \sum_{i=1}^{M_t} I_{i,j} x + v_j, \tag{1}$$

where η is the optical-to-electrical conversion coefficient, v_j is additive white Gaussian noise (AWGN) with zero mean and variance of $\sigma^2 = N_0/2$, i.e., $v_j \sim \mathcal{N}(0, \frac{N_0}{2})$. $I_{i,j}$ denotes the fading channel coefficient between the ith transmit aperture and jth receive aperture, and is subjected to the combined effects of turbulence-induced irradiance fluctuation and pointing errors. In [30], the authors indicated that the EGC diversity technique, when employed at the receiver, will provide a performance close to that of the optimal combining (OC) while having the advantage of implementation simplicity[1]. The signal at the output of

[1]The performance of OC is equivalent to that of MRC when there are no interfering signals at the receiver, as shown in [31].

the EGC receiver is expressed as

$$y = \eta \sum_{i=1}^{M_t} \sum_{j=1}^{N_r} I_{i,j} x + \sum_{j=1}^{N_r} v_j. \tag{2}$$

From (2), the electrical SNR of the combined signal is given by

$$\gamma_{EGC} = \frac{\eta^2 \mathbb{E}\left[|x|^2\right] \left(\sum_{i=1}^{M_t} \sum_{j=1}^{N_r} I_{i,j}\right)^2}{N_r \sigma^2} = \frac{\gamma_0 I_T^2}{N_r}, \tag{3}$$

where $\gamma_0 = \eta^2 \mathbb{E}[|x|^2]/\sigma^2$ denotes the average SNR and $I_T = \sum_{i=1}^{M_t} \sum_{j=1}^{N_r} I_{i,j}$. It can be seen from (3) that solving the distribution of I_T is the key to evaluate three important performance metrics (i.e., ergodic capacity, BER, and the outage performance) of MIMO FSO systems employing the EGC diversity technique.

B. Channel Model

The irradiance $I_{i,j}$ is considered to be the product of atmospheric turbulence-induced scintillation $I_{i,j}^a$ and pointing errors $I_{i,j}^p$, i.e., $I_{i,j} = I_{i,j}^a I_{i,j}^p$. As in [13], these two fading factors are approximately independent for smaller jitter values. In addition to this, it has been shown in [14] that the correlation time of the pointing errors induced by building sway, is on the order of a few seconds, which is bigger than that of the atmospheric turbulence (10–100 ms). Hence, both atmospheric turbulence and pointing errors can be considered to be independent. To characterize the fading $I_{i,j}^a$ over a wide range of turbulence conditions, the lognormal-Rician distribution model is adopted here as it provides an excellent fit with both simulation and experimental data in weak-to-strong turbulence regimes. The probability density function (PDF) of $I_{i,j}^a$ is given by [8]

$$f_{I_{i,j}^a}(h_a) = \frac{(1+r)\exp(-r)}{\sqrt{2\pi}\sigma_z} \int_0^\infty \frac{1}{z^2} I_0\left(2\sqrt{\frac{h_a r(1+r)}{z}}\right) \times \exp\left[-\frac{1+r}{z} - \frac{1}{2\sigma_z^2}\left(\ln(z) + \frac{1}{2}\sigma_z^2\right)^2\right] dz, \tag{4}$$

where $r \geq 0$ is the coherence parameter that represents the ratio of total power in the dominant or line-of-sight components to that of scattered components, σ_z^2 is the variance of the logarithm of the irradiance modulation factor z, and I_0 is the zero-order modified Bessel function of the first kind [32]. Note that (4) evolves from the product of a Rician amplitude and a lognormal modulation factor, i.e., $I_{i,j}^p = zy$. The PDFs of them are respectively expressed as

$$f_Z(z) = \frac{1}{\sqrt{2\pi}\sigma_z z} \exp\left[-\frac{1}{2}\left(\frac{\ln(z) + \frac{1}{2}\sigma_z^2}{\sigma_z}\right)^2\right]$$
$$f_Y(y) = (1+r)\exp(-r-(1+r)y)\, I_0\left(2\sqrt{r(1+r)y}\right). \tag{5}$$

From (5), it is easy to see the lognormal-Rician distribution comprises some well-known models as its special cases according to the different combinations of shape parameters. For example, the lognormal-Rician distribution reduces to the lognormal distribution as r approaches infinity. Also, it specialized to the lognormally modulated exponential distribution when r approaches 0.

Another performance limiting factor in FSO links is the pointing errors, which arise due to misalignment between the transmitter and receiver. It is noted that such effects are likely to occur in urban areas, where the FSO equipment is placed on high-rise structures [33], [34]. According to [14], the attenuation due to geometric spread and pointing errors can be approximated as

$$u(\rho) = I_{i,j}^p(\rho) \approx A_0 \exp\left(-2\frac{\rho^2}{w_{zeq}^2}\right),\ \rho \geq 0, \tag{6}$$

where $A_0 = [\mathrm{erf}(v)]^2$ is the fraction of the collected power at $\rho = 0$, $v = \sqrt{\pi} R_a/\sqrt{2} w_z$, R_a is the receiver's aperture radius, and w_z is the beam waist that can be approximated by $w_z = \theta z$ with θ denoting the transmit divergence angle. $w_{zeq} = \sqrt{w_z^2 \sqrt{\pi}\mathrm{erf}(v)/2v \exp(-v^2)}$ represents the equivalent beam waist. It must be mentioned that the approximation in (5) provides a good agreement with the exact value when the normalized beam width $w_z/R_a > 6$. For convenience, the independent identical Gaussian distributions for the elevation and the horizontal displacement (sway) are assumed, being σ_s^2 the jitter variance at the receiver. Thus, the PDF of radial displacement ρ follows a Rayleigh distribution, which is defined as [14]

$$f(\rho) = \frac{\rho}{\sigma_s^2} \exp\left(-\frac{\rho^2}{2\sigma_s^2}\right). \tag{7}$$

Combining (6) and (7), the probability distribution of $I_{i,j}^p$ becomes

$$f\left(I_{i,j}^p\right) = \frac{\xi^2}{A_0^{\gamma^2}} \left(I_{i,j}^p\right)^{\xi^2 - 1}, 0 \leq I_{i,j}^p \leq A_0, \tag{8}$$

where $\xi = w_{zeq}/2\sigma_s$.

III. An Efficient Approximation to the Distribution of I_T

A. Approximate Distribution for the Sum of L Random Variates

Based on the discussion of the previous section, we firstly deal with the challenges of the distribution of the sum of lognormal-Rician random variables (RVs) with pointing errors. For convenience, these channels are assumed to be statistically independent and identically distributed (i.i.d). The proposed methodology shown in the following has been partly introduced in [17], [35], where the distribution of the sum of independent Gamma-Gamma variates with and without pointing errors are investigated.

Let $\{I_l\}_{l=1}^L$ be a set of L i.i.d RVs that follows a lognormal-Rician with pointing errors distribution. Their sum is defined as

$$S = \sum_{l=1}^{L} I_l = \sum_{l=1}^{L} W_l u(r_l) = \sum_{l=1}^{L} z_l y_l u(r_l), \tag{9}$$

where $W_l = z_l y_l$, and $z_l, y_l, u(r_l)$, and r_l are lognormal, Rician, Rayleigh pointing errors, and Rayleigh RVs respectively. Note that (9) can be rewritten as

$$S = \frac{\sum_{l=1}^{L} z_l \sum_{l=1}^{L} y_l \sum_{l=1}^{L} u(r_l)}{L^2} + \frac{1}{L^2}\sum_{i=1}^{L-1}\sum_{j=i+1}^{L}(z_i - z_j) \times (y_i - y_j)\sum_{l=1}^{L} u(r_l) + \frac{1}{L}\sum_{i=1}^{L-1}\sum_{j=i+1}^{L}(z_i y_i - z_j y_j) \times (u(r_i) - u(r_j)). \quad (10)$$

Hence, according to (10), the unknown distribution S can be approximated by the distribution of the RV $\tilde{S}$, which is defined as the first term in (10), namely

$$S \approx \tilde{S} = \frac{\sum_{l=1}^{L} z_l \sum_{l=1}^{L} y_l \sum_{l=1}^{L} u(r_l)}{L^2}. \quad (11)$$

The summation of second and third terms in (10) represent the approximation error ϵ, which is given by

$$\begin{aligned}\epsilon &= \epsilon_1 + \epsilon_2 \\ &= \frac{1}{L^2}\sum_{i=1}^{L-1}\sum_{j=i+1}^{L}(z_i - z_j)(y_i - y_j)\sum_{l=1}^{L} u(r_l) \\ &\quad + \frac{1}{L}\sum_{i=1}^{L-1}\sum_{j=i+1}^{L}(z_i y_i - z_j y_j)(u(r_i) - u(r_j)). \end{aligned} \quad (12)$$

It can be easily seen from (12) that the ϵ goes to 0 for $L = 1$.

Next, we are now solving the distribution for RV $\tilde{S}$. Note that the sum of i.i.d lognormal variates can be efficiently approximated by an another lognormal distribution, as in [36]. Thus, the PDF of RV $G = \sum_{l=1}^{L} z_l$ is approximated as

$$f_G(g) \approx \frac{1}{\sqrt{2\pi\sigma_L^2}\, g} \exp\left[-\frac{(\ln(g) - \mu_L)^2}{2\sigma_L^2}\right], \quad (13)$$

where the parameters μ_L, σ_L^2 are respectively given by [36]

$$\begin{aligned}\sigma_L^2 &= \ln\left[\frac{\left(\exp\left(\sigma_z^2\right) - 1\right)}{L} + 1\right] \\ \mu_L &= \ln(L) - \frac{\sigma_L^2}{2}. \end{aligned} \quad (14)$$

Specifically, according to [37, TableIV], the right-hand-side of (13) can be expressed in terms of the Hermit polynomial representation. In this case, (13) can be rewritten as

$$f_G(g) \approx \frac{1}{\sqrt{\pi}}\sum_{k=1}^{K}\frac{w_k}{u_k}\mathbf{H}_{0,0}^{0,0}\left[\frac{g}{u_k}\middle|_{-}^{-}\right], \quad (15)$$

where $\mathbf{H}_{p,q}^{m,n}\left[\lambda\middle|_{(b_j,B_j)_{j=1:q}}^{(a_j,A_j)_{j=1:p}}\right]$ is the Fox's H function [38][2], $u_k = \exp(\sqrt{2}\sigma_L\omega_k + \mu_L)$, w_k and ω_k are the weight factor and zeros (abscissas) of the K-order Hermite polynomial [41]. In addition, the moment generating function (MGF) of $f_G(g)$ becomes [37], [42][3]

$$M_G(s) = \frac{1}{\sqrt{\pi}}\sum_{k=1}^{K} w_k \exp\left(-u_k s\right). \quad (16)$$

The effect of parameters K on the truncation errors of Gauss-Hermit quadrature rule integration is shown in [43]. Specifically, $K = 15$ is sufficient to achieve numerical accuracy, as shown in [42], where the performances of wireless communication systems are investigated in lognormal fading conditions [42], [44], [45].

Moreover, it is shown in [46] that the squared Rician distribution is actually a special case of $\kappa - \mu$ distribution with $\kappa = r, \mu = 1, \Omega = 1$. Hence, invoked by the [47], which demonstrates that the sum of L i.i.d $\kappa - \mu$ RVs with parameters $\kappa = r, \mu, \Omega$ is also a $\kappa - \mu$ RV with parameters $\kappa = r, L\mu, L\Omega$. Then, the PDF of RV $V = \sum_{l=1}^{L} y_l$ can be approximated as

$$f_V(v) \approx \frac{L(1+r)^{\frac{L+1}{2}} v^{\frac{L-1}{2}}}{\exp(Lr) r^{\frac{L-1}{2}} L^{\frac{L+1}{2}}} \exp\left(-(1+r)v\right) \times I_{L-1}\left(2\sqrt{r(1+r)vL}\right). \quad (17)$$

The above formula can be rewritten as

$$\begin{aligned} f_V(v) &\approx \sum_{q=0}^{Q}\frac{(rL)^q}{q!\Gamma(L+q)v}((1+r)v)^{L+q} \times \exp\left(-rL - (1+r)v\right) + R_Q(v) \\ &\approx \sum_{q=0}^{Q}\frac{\exp(-rL)(rL)^q}{l!\Gamma(L+q)}(1+r)^{L+q} v^{L+q-1} \times \mathbf{H}_{0,1}^{1,0}\left[(1+r)v\middle|_{0,1}^{-}\right] \\ &\approx \sum_{q=0}^{Q}\frac{\exp(-rL)(rL)^q}{q!\Gamma(L+q)}(1+r) \times \mathbf{H}_{0,1}^{1,0}\left[(1+r)v\middle|_{L+q-1,1}^{-}\right], \end{aligned} \quad (18)$$

where in (18), we have applied the series expansion result onto the I_{L-1} [32, eqn. (8.445)], and expressed the $\exp(\cdot)$ in terms of the Fox's H function [48, eqn. (2.5)]. The last equality in (18) holds due to [48, eqn. (2.4)]. The symbol $R_Q(v)$ in (18) denotes the truncation error, and is expressed as

$$R_Q(v) = \sum_{q=Q+1}^{\infty}\frac{(rL)^q}{q!\Gamma(L+q)v}((1+r)v)^{L+q} \times \exp\left(-rL - (1+r)v\right). \quad (19)$$

[2]The implementation of the univariate Fox's H function is reported in [39], [40] at Matlab or Mathematica.

[3]For a continuous positive random variable X, its MGF is defined as $M_X(s) = \int_0^\infty \exp(-sx) f_X(x) dx$, where $f_X(x)$ is the PDF of X.

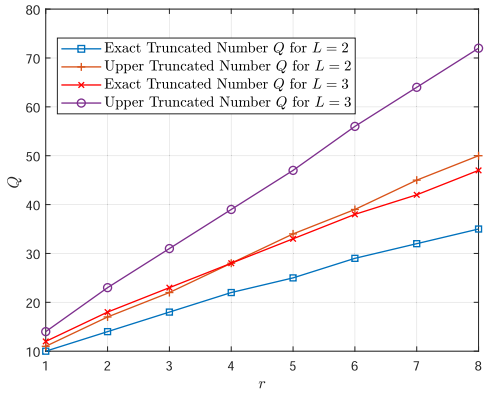

Fig. 1. The least truncated number Q that achieves the maximum error $\varepsilon = 10^{-5}$.

Theorem 1: When the truncated number Q is large enough, the truncation error $R_N(v)$ is upped bounded by

$$R_Q(v) < \frac{(1+r)}{2\pi Q}\left(\frac{rL\exp(1)}{Q+1}\right)^{Q+1}. \tag{20}$$

Proof: See Appendix A.

Fig. 1 presents the least values of truncated number Q for a given maximum error $\varepsilon = 10^{-5}$ under different scenarios. The exact and upper Q are derived according to $R_N(v)$ and the right-hand-side of (20). From this figure, we find that both of them nearly increase linearly with the value r, and they are close to each other for small r. Also, it can be found that $Q = 50$ is sufficient to guarantee the accuracy over a wide range of channel conditions.

Combining (15) and (18), the probability distribution for the RV $T_1 = \frac{1}{L}VG$ is obtained as

$$f_{T_1}(t_1) \approx \frac{1}{\sqrt{\pi}}\sum_{q=0}^{Q}\sum_{k=1}^{K}\frac{w_k}{u_k}\frac{L\exp(-rL)(rL)^q}{q!\Gamma(L+q)}(1+r) \times \mathbf{H}_{0,1}^{1,0}\left[\frac{(1+r)\,t_1\,L}{u_k}\middle|_{(L+q-1,1)}^{-}\right], \tag{21}$$

where we have used the [48, Theorem. (4.1)] in the above formula. Moreover, (21) can be further reduced to

$$f_{T_1}(t_1) \approx \frac{1}{\sqrt{\pi}}\sum_{q=0}^{Q}\sum_{k=1}^{K}w_k\frac{\exp(-rL)(rL)^q}{q!\Gamma(L+q)}\left(\frac{(1+r)\,L}{u_k}\right)^{L+q} \times t_1^{L+q-1}\exp\left(-\left(\frac{1+r}{u_k}\right)t_1\,L\right), \tag{22}$$

after using the following relation [49, eqn. (1.125)]

$$\mathbf{H}_{0,1}^{1,0}\left[z\middle|_{(b,B)}^{-}\right] = B^{-1}z^{\frac{b}{B}}\exp\left(-z^{\frac{1}{B}}\right). \tag{23}$$

Note that $T_2 = \frac{1}{L}\sum_{l=1}^{L}u(r_l) \approx Fu(\frac{1}{L}\sum_{l=1}^{L}r_l^2)$, and its PDF can be efficiently approximated by [17, eqn. (23)]

$$f_{T_2}(t_2) \approx (-1)^{L-1}\frac{L^L g^L}{t_2 2^L\Gamma(L)}\ln^{L-1}\left(\frac{t_2}{FA_0}\right)\left(\frac{t_2}{FA_0}\right)^{\frac{Lg}{2}}, \quad 0 \le t_2 \le FA_0, \tag{24}$$

where $g = w_{zeq}^2/2\sigma_s^2 = 2\xi^2$, $F = \frac{(2+gL)^L}{L^L g^{L-1}(2+g)}$ that satisfies $\lim_{g\to\infty}F = 1$ and $\lim_{L\to\infty}F = \exp(2/g)g/(g+2)$.

Consequently, the distribution of $\tilde{S} = T_1T_2$ is finally approximated by that of $\hat{S}$, which is found to be

$$f_{\tilde{S}}(s) \approx f_{\hat{S}}(s) \approx \frac{1}{\sqrt{\pi}}\sum_{q=0}^{Q}\sum_{k=1}^{K}w_k\frac{\exp(-rL)(rL)^q}{q!\Gamma(L+q)}\left(\frac{(1+r)}{u_kA_0F}L\right)^{\frac{Lg}{2}} \times \frac{L^Lg^L}{2^L}s^{\frac{Lg}{2}-1}G_{L,L+1}^{L+1,0}\left(\frac{s\,(1+r)}{u_kA_0F}L\middle|_{L+q-\frac{Lg}{2},(0)^{\otimes L}}^{(1)^{\otimes L}}\right), \tag{25}$$

where the notation $(\cdot)^{\otimes L}$ denotes the L times repetition of a given tuple, $G_{p,q}^{m,n}(\cdot|_{\ldots}^{\ldots})$ denotes the Meijer's G-function, and the definition of it is shown in Appendix D. A full derivation of (25) is given in Appendix B. Note that the derived approximate analytic solution of composite channel PDF in (25) facilitates the performance analysis of FSO systems and has not been obtained in the literature. Based on the discussion in Section III-A and extensive simulation studies, it is found that the truncated numbers $Q = 50$ and $K = 15$ are sufficient to achieve convergence for all of the numerical examples in the paper. Furthermore, by utilizing [50, eqn. (26)] and [32, eqn. (9.31.5)], the cumulative density function (CDF) of the combined fading can be approximated as

$$F_{\hat{S}}(a) \approx \frac{1}{\sqrt{\pi}}\sum_{q=0}^{Q}\sum_{k=1}^{K}w_k\frac{\exp(-rL)(rL)^q}{q!\Gamma(L+q)}\frac{L^Lg^L}{2^L} \times G_{L+1,L+2}^{L+1,1}\left(\frac{a\,(1+r)}{u_kA_0F}L\middle|_{L+q,\left(\frac{Lg}{2}\right)^{\otimes L},0}^{1,\left(1+\frac{Lg}{2}\right)^{\otimes L}}\right). \tag{26}$$

B. Approximation Error Analysis

Based on the information described above, the main ideas of our proposed approximate method are summarized as follows

$$S \approx \tilde{S} = \frac{\sum_{l=1}^{L}z_l\sum_{l=1}^{L}y_l\sum_{l=1}^{L}u(r_l)}{L^2} \approx \hat{S} = \frac{\phi\left(\sum_{l=1}^{L}z_l\right)\sum_{l=1}^{L}y_lFu\left(\sqrt{\frac{1}{L}\sum_{l=1}^{L}r_l^2}\right)}{L}, \tag{27}$$

where $\phi(\cdot)$ denotes some function. It should be noted that the value of RV $\phi(\sum_{l=1}^{L}z_l)$ in each generation extremely close to that of $(\sum_{l=1}^{L}z_l)$, and the PDF expression of $\phi(\sum_{l=1}^{L}z_l)$ is shown in (13). According to (27), the corresponding approximation error ϵ_t is given by

$$\epsilon_t = \epsilon + \left(\tilde{S} - \hat{S}\right). \tag{28}$$

Next, we make great efforts to analyze the ϵ_t. The exact PDF of the error ϵ_t is difficult to be derived, however, its first and second

moments, which are indicative of its statistical behavior [35], can be calculated. Hence, the mean of ϵ_t is derived as

$$\mathbb{E}\left[\epsilon_t\right] = \mathbb{E}\left[\epsilon\right] + \mathbb{E}\left(\tilde{S} - \hat{S}\right). \tag{29}$$

It is easy to see that the mean of ϵ is equal to 0 provided that the z_l, y_l, and $u(r_l)$ are statistically independent, and this indicates that $\hat{S}$ can be considered as a unbiased estimation of $\tilde{S}$. The means of $\tilde{S}$ and $\hat{S}$ are respectively obtained as

$$\mathbb{E}\left[\tilde{S}\right] = L\frac{A_0\xi^2}{1+\xi^2}, \tag{30}$$

and

$$\begin{aligned}\mathbb{E}\left[\hat{S}\right] &= \int_0^\infty f_{\hat{S}}(s)s ds \\ &= \frac{1}{\sqrt{\pi}}\sum_{q=0}^{Q}\sum_{k=1}^{K} w_k \frac{\exp\left(-rL\right)(rL)^q}{q!}\left(L+q\right)\frac{u_k A_0 F}{(1+r)L} \\ &\quad \times \frac{L^L g^L}{(Lg+2)^L} \\ &= \frac{1}{\sqrt{\pi}}\sum_{q=0}^{Q}\sum_{k=1}^{K} w_k \frac{\exp\left(-rL\right)(rL)^q}{q!}\left(L+q\right)\frac{u_k A_0}{(1+r)L} \\ &\quad \times \frac{\xi^2}{1+\xi^2}, \end{aligned} \tag{31}$$

where in (30) we have used the second equation in (70), and in (31) we have used the integration formula [17, eqn. (81)]. Using the Taylor series expansion of $\exp(x)$ at $x = 0$ [32, eqn. (1.211.1)], we have

$$\sum_{q=0}^{Q}\frac{(rL)^q}{q!}\left(L+q\right) \approx \exp(rL)L\left(r+1\right). \tag{32}$$

Knowing the fact that the first derivative of $M_G(s)$ at $s = 0$ is $-\mathbb{E}[G] = -L$. In other words, we have

$$-\left.\frac{dM_G(s)}{ds}\right|_{s=0} = L = \frac{1}{\sqrt{\pi}}\sum_{k=1}^{K} w_k u_k, \tag{33}$$

where the second equality holds due to (16). Then, we find that (31) reduces to (30) after substituting (32) and (33) into (31). In this case, we have

$$\mathbb{E}\left[\epsilon_t\right] = 0. \tag{34}$$

The variance of ϵ_t is given by

$$\mathbb{E}\left[\epsilon_t^2\right] = \mathbb{E}\left[\epsilon^2\right] + \mathbb{E}\left[\left(\tilde{S} - \hat{S}\right)^2\right], \tag{35}$$

where the variance of $\mathbb{E}[\epsilon^2]$ is obtained as

$$\begin{aligned}\mathbb{E}\left[\epsilon^2\right] &= \mathbb{E}[\epsilon_1^2] + \mathbb{E}[\epsilon_2^2] + 2\mathbb{E}\left[\epsilon_1\epsilon_2\right] \\ &= \mathbb{E}[\epsilon_1^2] + \mathbb{E}[\epsilon_2^2]. \end{aligned} \tag{36}$$

The second equation in (36) holds due to

$$\mathbb{E}\left[\left(\sum_{l=1}^{L} u(r_l)\right)\left(u(r_i) - u(r_j)\right)\right] = 0. \tag{37}$$

The variance of ϵ_1 and ϵ_2 are respectively derived as

$$\begin{aligned}\mathbb{E}\left[\epsilon_1^2\right] &= \frac{(L-1)}{L}\frac{(1+2r)}{(1+r)^2}\left(\exp\left(\sigma_z^2\right) - 1\right) \\ &\quad \times \left(\frac{A_0^2\xi^2}{2+\xi^2} + (L-1)\frac{A_0^2\xi^4}{(1+\xi^2)^2}\right), \end{aligned} \tag{38}$$

and

$$\begin{aligned}\mathbb{E}\left[\epsilon_2^2\right] &= (L-1)\left(\frac{2+4r+r^2}{(1+r)^2}\exp\left(\sigma_z^2\right) - 1\right) \\ &\quad \times \left(\frac{A_0^2\xi^2}{2+\xi^2} - \frac{A_0^2\xi^4}{(1+\xi^2)^2}\right). \end{aligned} \tag{39}$$

A full derivation of (38) and (39) is given in Appendix C. Also, the above two equations indicate that the variance of the approximation error increases for a certain combination of r, σ_z^2, A_0 and ξ as the number of RVs of the sum in (9) increases.

Proposition 1: The variance of ϵ is equal to that of ϵ_1 as ξ approaches ∞, which is given by

$$\mathbb{E}\left[\epsilon^2\right] = \mathbb{E}\left[\epsilon_1^2\right] = (L-1)\frac{(1+2r)}{(1+r)^2}\left(\exp\left(\sigma_z^2\right) - 1\right)A_0^2. \tag{40}$$

Proof: Proposition 1 can be easily proved according to $\lim_{\xi\to\infty}\mathbb{E}[\epsilon_2^2] = 0$.

Corollary 1: A more efficient approximation can be achieved for a larger ξ.

Proof: Substituting $A_0 = [\mathrm{erf}(\sqrt{\pi}R_a/\sqrt{2}w_z)]^2$ into (40) and using the relation $d\mathrm{erf}(x)/dx = 2\exp(-x^2)/\sqrt{\pi}$ [32, eqn. (8.250.1)], then the first derivative of $\mathbb{E}[\epsilon^2]$ is strictly less than zero according to (41).

$$\begin{aligned}\frac{d\mathbb{E}\left[\epsilon^2\right]}{dw_z/R_a} &= -(L-1)\frac{2(1+2r)}{(1+r)^2}\left(\exp\left(\sigma_z^2\right) - 1\right) \\ &\quad \times \mathrm{erf}\left(\sqrt{\pi/2}/(w_z/R_a)\right) \\ &\quad \times \frac{\sqrt{2}\exp\left(-\pi/2/(w_z/R_a)^2\right)}{(w_z/R_a)^2} \\ &< 0. \end{aligned} \tag{41}$$

The variance of $\mathbb{E}[(\tilde{S} - \hat{S})^2]$ is difficult to be solved since the function $\phi(\cdot)$ is unknown. However, it can be approximated with high accuracy in the following way

$$\begin{aligned}\mathbb{E}\left[\left(\tilde{S} - \hat{S}\right)^2\right] &\approx \left(\sum_{l=1}^{L} z_l \sum_{l=1}^{L} y_l\right)^2 \mathbb{E}\left[\left(\frac{1}{L^2}\sum_{l=1}^{L} u\left(r_l\right)\right.\right. \\ &\quad \left.\left. - \frac{F}{L}u\left(\sqrt{\frac{1}{L}\sum_{l=1}^{L} r_l^2}\right)\right)^2\right]. \end{aligned} \tag{42}$$

In Fig. 2, we investigate the tightness of the (36) and (40) by showing the numerical results. As can be seen, the variance of ϵ_1 approaches the variance of ϵ^2 as ξ increases. Specifically, they nearly overlap with each other for $w_z/R_a = 14, \sigma_s/R_a = 1$ ($\xi = 7.02$), and this verifies the argument of Proposition 1. In

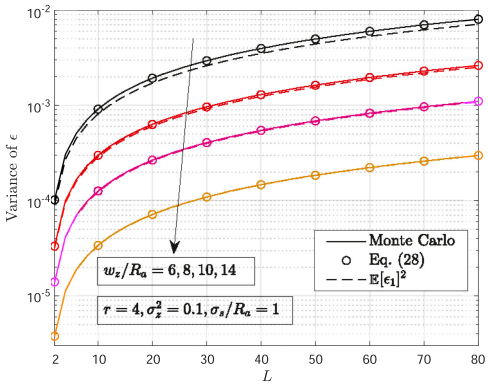

Fig. 2. The variance of ϵ for different pointing errors and L.

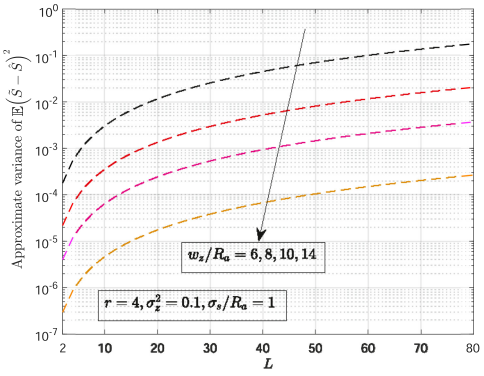

Fig. 3. Monte Carlo simulation results of approximate variance $\mathbb{E}[(\tilde{S}-\hat{S})^2]$ for different pointing errors and L.

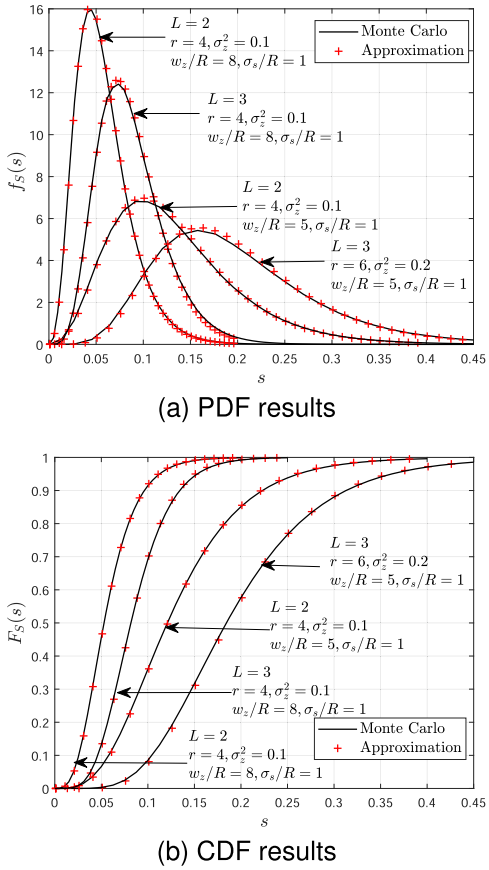

Fig. 4. PDF and CDF plots of the Monte Carlo simulation.

addition, we find that the variance of ϵ decreases with increasing value of w_z/R_a for given σ_s/R_a, and this is also shown in Fig. 3, where we presents the Monte Carlo simulation results of $\mathbb{E}[(\tilde{S}-\hat{S})^2]$. By comparing curves in Figs. 2 and 3, we conclude that a larger variance of approximation error is obtained when the number of apertures increase or w_z/R_a decreases.

C. Numerical Examples

In this section, we investigate the accuracy of the proposed approximate PDF expression by comparing the statistic of the simulation data. Note that the simulated PDFs and CDFs generalized from 1×10^6 samples by Monte Carlo method are used for reference. Fig. 4 depicts the PDF and CDF results for different combinations of turbulence conditions, apertures, and pointing errors. It is clearly illustrated that the approximate results always provide an excellent agreement with the simulation results.

To quantitatively evaluate the error behavior of the approximation method, we here employ the KS goodness-of-fit statistical tests tools, which measure the maximum value of absolute difference between the empirical cumulative distribution function (CDF) of the RV S, $F_S(\cdot)$ and the approximate analytical CDF expression $F_{\hat{S}}(\cdot)$ shown in (26). Hence, the KS test statistic is defined as

$$T = \max \left| F_S(a) - F_{\hat{S}}(a) \right|. \tag{43}$$

It is shown in [51] that an approximation is considered to be accepted with significance level $1-\alpha$ if the statistical test value T is less than given critical value $T_{\max}$, while it is said to be rejected with the same significance if $T > T_{\max}$. The critical value $T_{\max}$ is given by $T_{\max} = \sqrt{-\frac{1}{2N}\ln(\frac{\alpha}{2})}$ with α denoting the significant level and N is the number of samples. The typical value for them are set to be $\alpha = 5\%$ and $N = 10^4$ respectively, resulting in the critical value $T_{\max} = 0.0136$.

In Fig. 5, we study the KS test statistic of the approximation for different combinations of r, σ_z^2, w_z/R_a, σ_s/R_a and L. It must be emphasized that the present results are obtained by averaging the results of 100 simulation runs. According to Fig. 5, we find that the proposed approximation performs better for the larger r or smaller σ_z^2. Specifically, it is accepted with 95% significance in all the range of the parameters examined when $L = 2, w_z/R_a = 8, \sigma_s/R_a = 1$. The impact of pointing errors on the approximation accuracy can be concluded by comparing the curves in Fig. 5(a) and Fig. 5(b), which indicate that a more efficient approximation can be achieved for the smaller pointing errors. As expected, the number of apertures L have a negative effect on the approximation accuracy when comparing the statistic test results in Fig. 5(b) and Fig. 5(c).

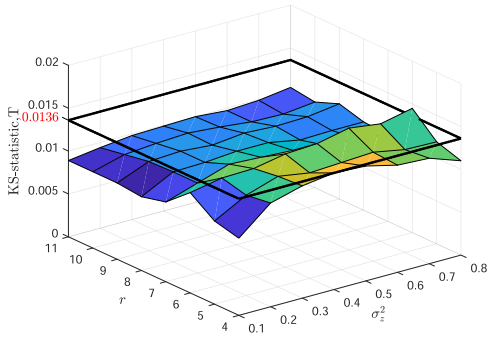

(a) $L = 2, w_z/R_a = 5, \sigma_s/R_a = 1.$

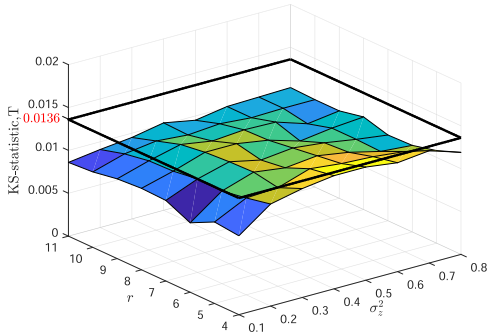

(b) $L = 2, w_z/R_a = 8, \sigma_s/R_a = 1.$

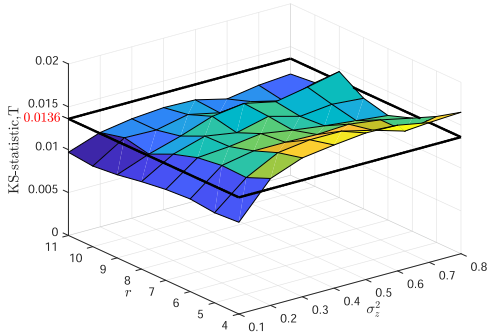

(c) $L = 3, w_z/R_a = 8, \sigma_s/R_a = 1.$

Fig. 5. KS goodness-of-fit tests results for different combinations of turbulence conditions, apertures, and pointing errors.

IV. Performance Analysis for the MIMO FSO Systems

In this section, we study the ergodic capacity, outage probability and BER performance of MIMO FSO systems over lognormal-Rician fading channels with pointing errors based on the proposed approximate model. In what follows, $L = M_t N_r$.

A. Ergodic Capacity

1) *Exact and asymptotic analysis:* Assuming the instantaneous channel side information is perfectly known at the receiver, the ergodic capacity corresponding to the considered MIMO FSO systems in bits/Hz/s is given by

$$C_{pe} = \mathbb{E}\left[\log_2\left(1 + \frac{\gamma_0}{N_r} s^2\right)\right]$$

$$= \int_0^\infty \frac{1}{\ln(2)} G_{2,2}^{1,2}\left(\gamma_0\, s^2 \Big|_{1,0}^{1,1}\right) f_S(s) ds$$

$$\approx \hat{C}_{pe} = \int_0^\infty \frac{1}{\ln(2)} G_{2,2}^{1,2}\left(\gamma_0\, s^2 \Big|_{1,0}^{1,1}\right) f_{\hat{S}}(s) ds, \quad (44)$$

where in (44), we have expressed $\ln(1+ax)$ in terms of Meijer's G-function [32, eqn. (8.4.6.5)]. Substituting (25) into (44) and using the integration formula [52], an approximate closed-form expression for the ergodic capacity of MIMO FSO communication systems is obtained as

$$C_{pe} \approx \frac{1}{\ln(2)\pi} \sum_{q=0}^{Q} \sum_{k=1}^{K} w_k \frac{\exp(-rL)(rL)^q}{q!\Gamma(L+q)} \frac{L^L g^L}{2^{L+1-q}}$$

$$\times\, G_{2\,L+4,2\,L+2}^{1,2\,L+4}\left(\frac{4\frac{\gamma_0}{N_r}}{\left(\frac{(1+r)}{u_k A_0 F} L\right)^2}\Bigg|_B^A\right), \quad (45)$$

where

$$A = \left\{1, 1, \frac{1-L-q}{2}, \frac{2-L-q}{2}, \left(\frac{2-\frac{Lg}{2}}{2}\right)^{\otimes L}\right\}$$

$$B = \left\{1, 0, \left(-\frac{Lg}{4}\right)^{\otimes L}\right\}. \quad (46)$$

It can be seen that the approximate expression in (45) involves the Meijer's G-function, and thus does not provide much insight into the capacity performance. Also, we are always interested in the ergodic capacity in the high SNR regime. Note that $\log_2(1+\gamma_0/N_r s^2)$ can be approximated by $\log_2(\gamma_0/N_r s^2)$ in this case. As such, we have

$$C_{pe,hsnr} \approx \int_0^\infty \log_2\left(\gamma_0/N_r s^2\right) f_S(s) ds$$

$$\approx \log_2(\gamma_0/N_r) + \int_0^\infty 2\log_2(s) f_{\hat{S}}(s) ds. \quad (47)$$

Substituting (25) into (47), we can obtain an asymptotic expression of ergodic capacity at high SNRs as

$$C_{pe,hsnr} \approx \frac{1}{\ln(2)}\Bigg(\frac{1}{\sqrt{\pi}} \sum_{q=0}^{Q} \sum_{k=1}^{K} w_k \frac{\exp(-rL)(rL)^q}{q!}$$

$$\left(-\frac{4}{g} + 2\varphi(0, L+q) + 2\ln\left(\frac{u_k A_0 F}{(1+r)L}\right)\right)$$

$$+ \ln\left(\frac{\gamma_0}{N_r}\right)\Bigg)$$

$$\approx \frac{1}{\ln(2)}\Bigg(2\sum_{q=0}^{Q} \frac{\exp(-rL)(rL)^q}{q!} \varphi(0, L+q)$$

$$- \frac{4}{g} - \sigma_L^2 + 2\ln\left(\frac{A_0 F}{(1+r)}\right) + \ln\left(\frac{\gamma_0}{N_r}\right)\Bigg), \quad (48)$$

where $\varphi(\cdot)$ is the digamma function [32, eqn. (8.365.4)] and we have used the following integration formula, i.e., (49) [17, eqn. (83)] in deriving the first equality of (48).

$$\int_0^\infty t^{q_1-1}\ln(t)G_{L,L+1}^{L+1,0}\left(t\middle|_{q_2,0,\ldots,0}^{1,\ldots,1}\right)dt = -\frac{L\Gamma(q_1+q_2)}{q_1^{L+1}}+\frac{\Gamma(q_1+q_2)\varphi(0,q_1+q_2)}{q_1^L}. \quad (49)$$

Note that (48) gives the required expression for the ergodic capacity at high SNRs in terms of simple elementary function. According to (48), the multiplexing gain[4] is computed to be 1, and a smaller variance σ_z^2 or larger g leads to a higher ergodic capacity. Specifically, $\sigma_L^2 \approx \sigma_z^2/L$ when σ_z^2 is small enough, and this indicates that the ergodic capacity at high SNRs decreases linearly with increasing variance σ_z^2. It should be emphasized that this conclusion can not be deduced directly by using the numerical methods, namely, Padé and Gram-Charlier Series. Knowing the fact that the effect of pointing errors can be neglected when $A_0 \to 1$ and $g \to \infty$ [15], then the approximate and the asymptotic expressions for the ergodic capacity of MIMO FSO systems in the absence of pointing errors are respectively evaluated as

$$C_{npe} \approx \frac{1}{\ln(2)\pi}\sum_{q=0}^{Q}\sum_{k=1}^{K} w_k \frac{\exp(-rL)(rL)^q}{q!\Gamma(L+q)}\frac{L^L g^L}{2^{L+1-q}} \times G_{4,2}^{1,4}\left(\frac{4\frac{\gamma_0}{N_r}}{\left(\frac{(1+r)}{u_k}L\right)^2}\middle|_{1,0}^{1,1,\frac{1-L-q}{2},\frac{2-L-q}{2}}\right), \quad (50)$$

and

$$C_{npe,hsnr} \approx \frac{1}{\ln(2)}\left(2\sum_{q=0}^{Q}\frac{\exp(-rL)(rL)^q}{q!}\varphi(0,L+q) - \sigma_L^2 - 2\ln(1+r) + \ln\left(\frac{\gamma_0}{N_r}\right)\right). \quad (51)$$

2) *Beam width optimization at high SNRs:* It is known that the beam width can be optimized to mitigate the effects of pointing error in the high SNR regime. According to [54], an SNR threshold, $\gamma_{th}[dB]$, is defined as a critical point that intersects with the γ_0-axis. Hence, from (48) and (51), we can obtain the expression of SNR loss caused by pointing errors as

$$\begin{aligned}\text{Loss}_{pe}\,[\text{dB}] &= \gamma_{th,pe}[\text{dB}] - \gamma_{th,npe}[\text{dB}] \\ &= -\frac{20}{\ln(10)}\ln\left(\exp(-2/g)A_0F\right) \quad (52)\end{aligned}$$

The above formula indicates that the optimum normalized beam $w_{z,opt}/R_a$ only depends on pointing errors and is obtained by solving following optimization problems

$$\begin{aligned}w_{z,opt}/R_a &= \max_{w_z/R_a\in(6,\infty)}\left(-2/g+\ln(A_0F)\right) \\ &= \max_{w_z/R_a\in(6,\infty)}\left(\exp(-2/g)A_0F\right) \quad (53)\end{aligned}$$

Specifically, when L is large enough, (53) reduces to

$$w_{z,opt}/R_a = \max_{w_z/R_a\in(6,\infty)}\left(A_0\frac{g}{g+2}\right) \quad (54)$$

Using the formula in [55, eqn. (24)], we then find the objective function in (54) decreases monotonically as w_z/R_a increases, and this indicates $w_{z,opt}/R_a = 6$.

B. Outage Performance

Outage probability is also an important performance metric, which is defined as the probability that the instantaneous combined SNR γ_{EGC} is lower than a given threshold γ_{th}, that is

$$P_{out,pe} = \Pr(\gamma_{EGC} < \gamma_{th}) \approx \int_0^{\sqrt{\frac{N_r\gamma_{th}}{\gamma_0}}} f_{\hat{S}}(s)ds. \quad (55)$$

Substituting (25) into (55) and using (26), the outage performance for the MIMO FSO systems with pointing errors can be approximated as

$$P_{out,pe} \approx \frac{1}{\sqrt{\pi}}\sum_{q=0}^{Q}\sum_{k=1}^{K} w_k \frac{\exp(-rL)(rL)^q}{q!\Gamma(L+q)}\frac{L^L g^L}{2^L} \times G_{L+1,L+2}^{L+1,1}\left(\frac{\sqrt{\frac{N_r\gamma_{th}}{\gamma_0}}(1+r)}{u_kA_0F}L\middle|_{L+q,\left(\frac{Lg}{2}\right)^{\bigotimes L},0}^{1,\left(1+\frac{Lg}{2}\right)^{\bigotimes L}}\right). \quad (56)$$

Correspondingly, an approximate analytic expression for the outage performance of MIMO FSO systems without pointing errors can be readily carried out by

$$\begin{aligned}P_{out,npe} &\approx \frac{1}{\sqrt{\pi}}\sum_{q=0}^{Q}\sum_{k=1}^{K} w_k \frac{\exp(-rL)(rL)^q}{q!\Gamma(L+q)} \times G_{1,2}^{1,1}\left(\frac{\sqrt{\frac{N_r\gamma_{th}}{\gamma_0}}(1+r)}{u_k}L\middle|_{L+q,0}^{1}\right) \\ &\approx \frac{1}{\sqrt{\pi}}\sum_{q=0}^{Q}\sum_{k=1}^{K} w_k \frac{\exp(-rL)(rL)^q}{q!\Gamma(L+q)} \times \gamma\left(L+q,\left(\frac{1+r}{u_k}\right)L\sqrt{\frac{N_r\gamma_{th}}{\gamma_0}}\right), \quad (57)\end{aligned}$$

where $\gamma(\cdot,\cdot)$ denotes the lower incomplete gamma function [32, eqn. (8.35)] and the second equality in (57) holds due to [56].

[4]The multiplexing gain of a system is defined as $\lim_{\gamma_0\to\infty}\frac{C(\gamma_0)}{\log_2(\gamma_0)}$, where C and γ_0 represent the channel ergodic and SNR respectively [53].

C. BER Performance

1) *Exact analysis:* For an FSO system using OOK modulation scheme, the average BER performance is given by [57]

$$P_{b,pe} = \mathbb{E}\left[\frac{1}{2}\text{erfc}\left(\sqrt{\frac{\gamma_0\, s^2}{4N_r}}\right)\right] \approx \frac{1}{2\sqrt{\pi}}\int_0^\infty f(\hat{s}) G_{1,2}^{2,0}\left(\frac{\gamma_0}{4N_r}\hat{s}^2\Big|_{0,0.5}^{1}\right) d\hat{s}, \quad (58)$$

where in (58), erfc$(\cdot)$ denotes the complementary error function [32, eqn. (8.250.4)], and it is expressed in terms of Meijer's G-function [58, eqn. (8.4.14.1)]. Substituting (25) into (58) and using the integration formula [52], an approximate closed-form expression for the BER performance of MIMO FSO communication systems is obtained as

$$P_{b,pe} \approx \frac{1}{\pi^{\frac{3}{2}}}\sum_{q=0}^{Q}\sum_{k=1}^{K} w_k \frac{\exp(-rL)(rL)^q}{q!\Gamma(L+q)}\frac{L^L g^L}{2^L} 2^{q-2} \times G_{L+3,L+2}^{2,L+2}\left(\frac{\gamma_0}{N_r\left(\frac{(1+r)}{u_k A_0 F}L\right)^2}\Bigg|_{0,0.5,\left(-\frac{Lg}{4}\right)^{\otimes L}}^{\frac{1-L-q}{2},\frac{2-L-q}{2},\left(1-\frac{Lg}{4}\right)^{\otimes L},1}\right). \quad (59)$$

Correspondingly, an approximate analytic expression for the BER performance of MIMO FSO systems without pointing errors is obtained as

$$P_{b,npe} \approx \frac{1}{\pi^{\frac{3}{2}}}\sum_{q=0}^{Q}\sum_{k=1}^{K} w_k \frac{\exp(-rL)(rL)^q}{q!\Gamma(L+q)} 2^L 2^{q-2} \times G_{3,2}^{2,2}\left(\frac{\gamma_0}{N_r\left(\frac{(1+r)}{u_k}L\right)^2}\Bigg|_{0,0.5}^{\frac{1-L-q}{2},\frac{2-L-q}{2},1}\right). \quad (60)$$

2) *Diversity Order and Coding Gain:* At high SNRs, the average BER performance can be approximated as $P_b \approx (G_c\gamma_0)^{-G_d}$, where G_c and G_d are defined as coding gain and diversity respectively. In a log-log scale, the diversity gain G_d determines the slope of the BER versus SNR curves while coding gain G_d specifies a relative horizontal shift to a benchmark BER curve of $(\gamma_0)^{-G_d}$. Note that the relationship $\xi^2 > 1$ always holds in most practical FSO systems [15], [55]. Hence, by utilizing (78) in Appendix D and after some algebraic manipulations, the asymptotic BER performance can be obtained as

$$P_{b,pe,asym} \approx \sum_{k=1}^{K}\frac{w_k}{\pi}\frac{\exp(-rL)}{\Gamma\left(\frac{L}{2}\right)}\xi^{2L}\left(\frac{\gamma_0}{N_r\left(\frac{(1+r)}{u_k A_0 F}L\right)^2}\right)^{-L/2} \times \frac{\Gamma\left(\frac{1}{2}\right)}{L(\xi^2-1)^L}. \quad (61)$$

TABLE I
FSO SYSTEMS CONFIGURATION PARAMETERS

Parameter	Symbol	Value
Wavelength	λ	1550 nm
Wavenumber	κ	$2\pi/\lambda$
Source-destination link distance	d_{SD}	5 km
Receiver aperture diameter	$D = 2R_a$	10 cm
Transmit divergence at $1/e^2$	θ_z	0.66mrad
Beam width at 5 km	ω_z	≈ 330 cm
Jitter angle at $1/e^2$	θ_s	0.11mrad
Maximum jitter at 5 km	σ_s	≈ 55 cm
Refractive index structure parameter	C_n^2	$1\times10^{-14}\text{m}^{-2/3}$

From (61), the diversity order and coding gain are found to be

$$G_d = L/2$$

$$G_c = \left(\frac{1}{\pi}\sum_{k=1}^{K} w_k u_k^{-L} L^{L-1}\Gamma\left(\frac{1}{2}\right)\frac{1}{\Gamma\left(\frac{L}{2}\right)}\right)^{-2/L} \times \left(\frac{(A_0F)^2\exp(2r)\left(1-\frac{1}{\xi^2}\right)^2}{N_r(1+r)^2}\right). \quad (62)$$

V. NUMERICAL RESULTS AND DISCUSSION

In this section, we present some numerical results for the ergodic capacity, outage probability and BER performance of MIMO FSO systems over lognormal-Rician turbulence channels with pointing errors. The Monte Carlo simulation results are obtained through MATLAB, and they are also included as a benchmark in all the figures. A detailed description of Monte Carlo simulation is present as follows: For given channel model parameters $\gamma_0, M_t, N_r, r, \sigma_z^2, w_z/R_a, \sigma_s/R_a$, we generate N i.i.d Lognormal-Rician RVs with pointing errors, and repeat this $M_t \times N_r$ times. Then, substituting these RVs into (44), (55) and (58), we arrive at the Monte Carlo simulation results of ergodic capacity, outage probability and BER performance respectively.

Moreover, the number of samples N is set to be 10^6 if not specified yet. The system configuration parameters in all the simulations are listed in Table I. Note that these parameters have been used in most practical FSO systems [15], [55]. The values of lognormal-Rician turbulence parameters (r, σ_z^2) are adopted according to [21], [24], [59]. It is shown in [15] that $\rho_0 = 0.79\,(C_n^2\kappa^2 d_{SD})^{-3/5}$ for a plane wave propagation, and thus a spacing of 14 mm is required to achieve uncorrelated fading when using the parameters in Table I.

Fig. 6 depicts the simulated, approximate analytical, and high SNR ergodic capacity of MIMO FSO systems as a function of the average electrical SNR γ_0 for different apertures and pointing errors. Note that the pointing errors are considered here assuming values of normalized beam width and normalized jitter of $(w_z/R_a = 5, \sigma_z/R_a = 1)$, and $(w_z/R_a = 10, \sigma_z/R_a = 2)$. From the figure, we illustrate that the approximate analytical expression in (45) and asymptotic expression in (47) are in excellent agreement with the Monte Carlo simulation results, and thus verify the high accuracy of the proposed approximation. Also,

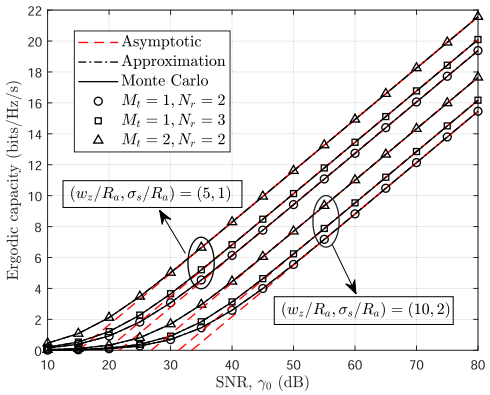

Fig. 6. The ergodic capacity of MIMO FSO systems for different combinations of apertures and pointing errors when $r = 4, \sigma_z^2 = 0.1$.

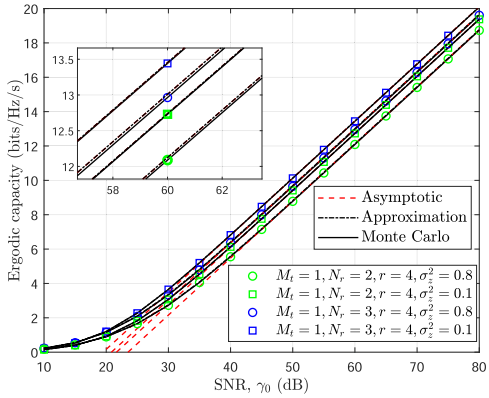

Fig. 7. The ergodic capacity of SIMO FSO systems for different combinations of turbulence conditions and apertures when $w_z/R_a = 5, \sigma_s/R_a = 1$.

TABLE II
THE ERGODIC CAPACITY OF MIMO FSO SYSTEMS WITH $M_T = N_r = 3$, WHERE RELATIVE ERROR δ IS DEFINED AS $\delta = |C_{pe} - \hat{C}_{pe}|/C_{pe}$

SNR(dB)	C_{pe} (bits/Hz/s)	$\hat{C}_{pe}$ (bits/Hz/s)	δ
0	0.1698	0.1661	0.0218
10	1.1307	1.1129	0.0157
20	3.6310	3.5869	0.0121
30	6.8311	6.7535	0.0114
40	10.1401	10.0273	0.0111
50	13.4608	13.3126	0.0110
60	16.7826	16.5991	0.0109
70	20.1045	19.8857	0.0109
80	23.4264	23.1723	0.0108

TABLE III
A COMPARISON OF ASYMPTOTIC ERGODIC CAPACITY FOR SISO FSO SYSTEMS

SNRdB	Monte Carlo	Moment-Based	Series Representation
45	9.3525	9.2773	9.9871
50	10.9795	10.9383	11.6372
55	12.6222	12.5993	13.2930
60	14.2733	14.2602	14.9515
65	15.9253	15.9212	16.6113
70	17.5847	17.5822	18.2717
75	19.2478	19.2431	19.9324
80	20.9057	20.9041	21.5932

it must be highlighted that the obtained analytical expression of ergodic capacity is very precise in the entire SNR regime, that is, overlaps with the simulation results from low to high SNR. As expected, the ergodic capacity is significantly increased as the apertures increase. For example, when $(w_z/R_a = 10, \sigma_z/R_a = 2)$ and $\gamma_0 = 50$ dB, the ergodic capacity for $M_t = 1, N_r = 2$ is 5.54 bits/Hz/s while it is 7.68 bits/Hz/s for $M_t = 2, N_r = 2$. In other words, the impacts of pointing errors can be mitigated greatly by utilizing the MIMO technique.

Furthermore, the results presented in Table II show that the obtained approximate expressions are also efficient for the MIMO FSO systems with larger apertures at both ends and the relative error decreases as SNR increases. In Table III, we present a comparison of asymptotic ergodic capacity between series representation method and moment-based method for the SISO cases. It can be easily seen from the table that the asymptotic

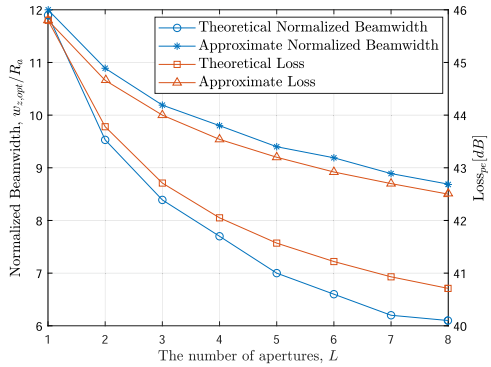

Fig. 8. The effects of apertures on the optimum normalized beam width in the high SNR regime when $r = 4, \sigma_z^2 = 0.1, \sigma_s/R_a = 6$.

ergodic capacity results obtained by using the moment-based method are closer to the Monte Carlo results and this is because of the fact that moment-based method is equivalent to solve $\mathbb{E}[\log_2(1 + \gamma_0 s^2)]$ at high SNRs from the perspective of methodology. More specifically, the results obtained by the series representation method is around 3% more than those obtained by the moment-based method.

The impacts of turbulence conditions and apertures on the ergodic capacity of SIMO FSO systems are investigated in Fig. 7. By comparing these curves, we find the smaller variance σ_z^2 results in larger ergodic capacity. For example, when $M_t = 1, N_r = 2$, and $\gamma_0 = 50$ dB, the ergodic capacity for $\sigma_z^2 = 0.1$ is 9.41 bits/Hz/s while it is 8.78 bits/Hz/s for $\sigma_z^2 = 0.8$. As expected, the ergodic capacity can be improved with the increasing number of the apertures.

Fig. 8 presents the effects of number of apertures on the optimum normalized beam width at high SNRs. Note that the theoretical normalized beamwidth and loss are derived from the Monte Carlo simulation while the approximate results are derived from (53). From this figure, we find that the obtained approximate results act as a upper bound when compared with the theoretical results except for the SISO cases, where they almost overlap with each other. Also, it can be easily seen

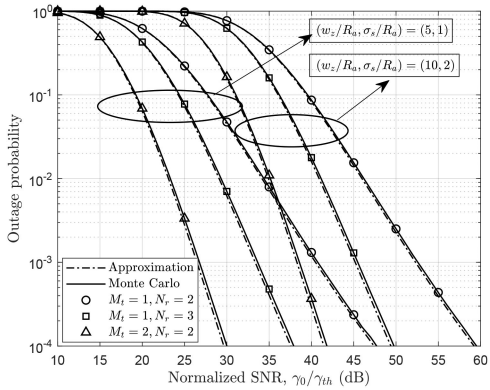

Fig. 9. The outage probability of MIMO FSO systems for different combinations of apertures and pointing errors when $r = 4, \sigma_z^2 = 0.1$.

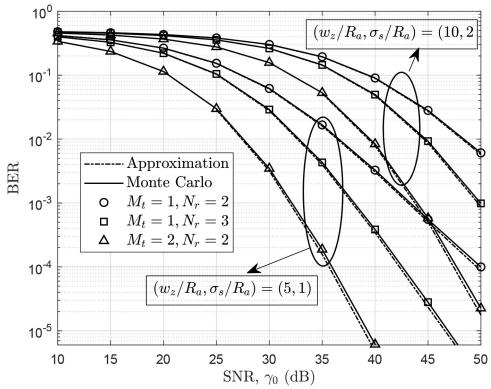

Fig. 10. The BER performance of MIMO FSO systems for different combinations of apertures and pointing errors when $r = 4, \sigma_z^2 = 0.1$.

that both the optimum normalized beam width and SNR loss decrease slowly as L increases, and this indicates that L is much greater than 8 to achieve the validity of (54) for the considered channel model. For example, the optimum beamwidth derived from (53) is $w_{z,opt}/R_a = 6.7$ when L is 30.

The outage performance of MIMO FSO systems over lognormal-Rician turbulence channels with pointing errors is shown in Fig. 9. As can be seen, the analytical expression in (56) provides an excellent match in the low-to-medium SNR regime while it acts as a lower bound at high SNRs. However, we note that it also can be regarded as a reasonable reference to the actual system performance since the simulation results lie within 0.3 dB in all cases examined. As expected, the outage performance is significantly improved as the apertures increase.

Fig. 10 depicts the BER performance of MIMO FSO systems for the considered channel models. It can be seen that the obtained approximate results almost overlap with the simulation results in the low-to-medium SNR regime while it acts as a lower bound at high SNRs, and this is consistent with the results shown for the outage performance. Also, the asymptotic BER performance in Fig. 11 verifies the expressions in (61) and (62).

Overall, in all of the cases considered, we find that there is a good match between the approximate analytical and the simulated results, and this implies that the proposed method is

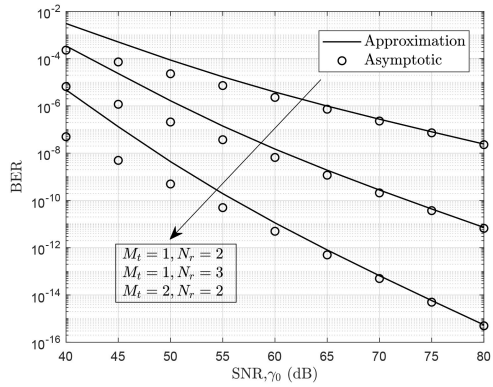

Fig. 11. Asymptotic BER performance of MIMO FSO systems for different numbers of apertures when $r = 4, \sigma_z^2 = 0.1, w_z/R_a = 5, \sigma_s/R_a = 1$.

highly efficient to approximate the PDF of sum of Lognormal-Rician RVs with pointing errors over a wide range of channel conditions. Moreover, our new method can also be applied to evaluate the performance of MIMO wireless communication systems over other composite lognormal-X fading channels, such as gamma-lognormal and weibull-lognormal, which are widely used to describe the statistical properties of wireless communication channels in congested downtown areas and in satellite communication systems [60], [61].

VI. Conclusion

In this paper, we have discussed the performance of MIMO FSO systems employing the EGC scheme over lognormal-Rician turbulence channels with pointing errors. A novel approximate analytical PDF expression for the considered channel model is developed. The KS test results indicate that the proposed approximation is highly accurate over a wide range of channel conditions. Based on the obtained statistical formulas, the closed-form expressions for the ergodic capacity, outage probability, and BER performance are formulated. The derived analytical expression of ergodic capacity is shown to be in excellent agreement with the Monte Carlo simulation results over the whole SNR regime. The obtained asymptotic ergodic capacity not only enables us to gain insights into the impacts of the system parameters, but also helps us to formulate beam width optimization at the transmitter side. Moreover, it can be observed that the obtained approximate results for the outage probability and BER performance are very tight in the low-to-medium SNR regime, while they act as a lower bound in the high SNR regime.

Appendix A

$$R_Q(v) < \sum_{q=Q+1}^{\infty} \frac{(rL)^q}{q!\Gamma(L+q)} (1+r)^{L+q} \left(\frac{L+q-1}{1+r} \right)^{L+q-1} \times \exp\left(-rL - (L+q-1)\right) < \sum_{q=Q+1}^{\infty} \frac{(rL)^q}{q!\Gamma(L+q)} (1+r)(L+q-1)^{L+q-1}$$

$$\begin{aligned}
&\times \exp\left(-rL-(L+q-1)\right)\\
&< \sum_{q=Q+1}^{\infty} \frac{(rL)^q}{q!}(1+r)\frac{\exp\left(L+q-1\right)}{\sqrt{2\pi\left(L+q-1\right)}}\\
&\times \exp\left(-rL-(L+q-1)\right)\\
&< \frac{(rL)^{Q+1}(1+r)}{(Q+1)!\sqrt{2\pi\left(L+Q\right)}}\frac{Q+2}{Q+2-rL}\\
&\times \exp\left(-rL\right)\\
&< \frac{(1+r)}{\sqrt{2\pi\left(Q+1\right)}\sqrt{2\pi\left(L+Q\right)}}\left(\frac{rL\exp(1)}{Q+1}\right)^{Q+1}.
\end{aligned} \tag{63}$$

where in (63), the first equality holds according to (64), which indicates that $u=n/(1+r)$ maximizes $v^{L+q-1}\exp(-(1+r)v)$ regardless of r,n.

$$\frac{dv^{L+q-1}\exp\left(-\left(1+r\right)v\right)}{dv}=0\Rightarrow v=\frac{L+q-1}{1+r}. \tag{64}$$

The Stirling asymptotic formula [32, eqn. (8.327.2)] can be applied to derive the third and fifth inequalities provided that Q is large enough. In addition, the fourth inequality holds due to

$$\begin{aligned}
\sum_{q=Q+1}^{\infty}\frac{(rL)^q}{q!} &= \frac{(rL)^{Q+1}}{(Q+1)!}\left(1+\frac{rL}{Q+2}+\frac{(rL)^2}{(Q+2)(Q+3)}\right.\\
&\left.+\frac{(rL)^3}{(Q+2)(Q+3)(Q+4)}\cdots\right)\\
&< \frac{(rL)^{Q+1}}{(Q+1)!}\left(1+\frac{rL}{Q+2}+\frac{(rL)^2}{(Q+2)^2}\right.\\
&\left.+\frac{(rL)^3}{(Q+2)^3}+\cdots\right)\\
&< \frac{(rL)^{Q+1}}{(Q+1)!}\frac{Q+2}{Q+2-rL}, \text{if } Q+2>rL.
\end{aligned} \tag{65}$$

APPENDIX B

To derive the (25), we mainly focus on solving the following integral:

$$\begin{aligned}
&\int_{\frac{s}{FA_0}}^{\infty}\frac{1}{y}t_1^{L+q-1}\exp\left(-\frac{1+r}{u_k}t_1L\right)\ln^{L-1}\left(\frac{FA_0t_1}{s}\right)\\
&\times\left(\frac{s}{t_1FA_0}\right)^{\frac{Lg}{2}}dt_1.
\end{aligned} \tag{66}$$

Performing the change of variable $\frac{FA_0t_1}{s}=h$, (66) can be rewritten as

$$\begin{aligned}
&\int_1^{\infty}\frac{1}{FA_0}\left(\frac{y}{FA_0}\right)^{L+q-1}h^{L+q-\frac{Lg}{2}-1}\\
&\times\exp\left(-\frac{1+r}{u_k}\frac{s}{FA_0}Lh\right)\ln^{L-1}(h)dh.
\end{aligned} \tag{67}$$

Note that the integral involving in (67) can be evaluated as

$$\begin{aligned}
&\int_1^{\infty}h^{L+q-\frac{Lg}{2}-1}\exp\left(-\frac{1+r}{u_k}\frac{s}{FA_0}Lh\right)\ln^{L-1}(h)dh\\
&=\Gamma(L)\left(\frac{1+r}{u_k}\frac{s}{FA_0}L\right)^{\frac{Lg}{2}-(L+q)}\\
&\times G_{L,L+1}^{L+1,0}\left(\frac{s\left(1+r\right)}{u_kA_0F}L\Big|_{L+q-\frac{Lg}{2},0,\ldots,0}^{1,\ldots,1}\right),
\end{aligned} \tag{68}$$

where in (68), we have used the following integration formula [17, eqn. (79)]

$$\begin{aligned}
&\int_1^{\infty}x^{v-1}\exp\left(-tx\right)\ln^m(x)dx\\
&=\Gamma\left(m+1\right)t^{-v}G_{m+1,m+2}^{m+2,0}\left(t\Big|_{v,0,\ldots,0}^{1,\ldots,1}\right).
\end{aligned} \tag{69}$$

Hence, combining (22), (24), and (68) yields (25) after some algebraic manipulations.

APPENDIX C

Since $\{z_l\}_{l=1}^{l=L}$, $\{y_l\}_{l=1}^{l=L}$, and $\{u(r_l)\}_{l=1}^{l=L}$ are identically distributed variates with parameters (σ_z^2), (r), and (A_0,ξ); their first moments and variances are given by

$$\begin{aligned}
\mathbb{E}\left[z_l\right]&=\mathbb{E}[y_l]=1\\
\mathbb{E}\left[u(r_l)\right]&=\frac{A_0\xi^2}{1+\xi^2}\\
\mathbb{E}\left[z_l^2\right]&=\exp\left(\sigma_z^2\right)\\
\mathbb{E}\left[y_l^2\right]&=\frac{(2+r(4+r))}{(1+r)^2}\\
\mathbb{E}\left[u^2(r_l)\right]&=\frac{A_0^2\xi^2}{2+\xi^2}.
\end{aligned} \tag{70}$$

The variance of ϵ_1 and ϵ_2 are equal to their second moments individually, which are respectively given by

$$\begin{aligned}
\mathbb{E}\left[\epsilon_1^2\right]&=\frac{1}{L^4}\mathbb{E}\left[\left(\sum_{i=1}^{L-1}\sum_{j=i+1}^{L}\left(z_i-z_j\right)\left(y_i-y_j\right)\right)^2\right]\\
&\times\mathbb{E}\left[\left(\sum_{l=1}^{L}u(r_l)\right)^2\right],
\end{aligned} \tag{71}$$

and

$$\begin{aligned}
\mathbb{E}\left[\epsilon_2^2\right]&=\frac{1}{L^2}\mathbb{E}\left[\left(\sum_{i=1}^{L-1}\sum_{j=i+1}^{L}\left(z_iy_i-z_jy_j\right)\right.\right.\\
&\left.\left.\times\left(u(r_i)-u(r_j)\right)\right)^2\right].
\end{aligned} \tag{72}$$

$$\mathbb{E}\left[\left(W_i - W_j\right)\left(u(r_i) - u(r_j)\right)\left(W_g - W_h\right)\left(u(r_g) - u(r_h)\right)\right] = \begin{cases} 4\left(\frac{2+4r+r^2}{(1+r)^2}\exp\left(\sigma_z^2\right) - 1\right)\left(\frac{A_0^2\xi^2}{2+\xi^2} - \frac{A_0^2\xi^4}{(1+\xi^2)^2}\right) & \text{if } i = g \text{ and } j = h \\ 0 & \text{if } i \neq g \text{ and } j \neq h \\ \left(\frac{\left(2+4r+r^2\right)}{(1+r)^2}\exp\left(\sigma_z^2\right) - 1\right)\left(\frac{A_0^2\xi^2}{2+\xi^2} - \frac{A_0^2\xi^4}{(1+\xi^2)^2}\right) & \text{if } i = g \text{ and } j \neq h \end{cases} \tag{75}$$

Using the second and fifth equalities in (70), (71) is then transformed into

$$\mathbb{E}\left[\epsilon_1^2\right] = \frac{1}{L^3}\mathbb{E}\left[\left(\sum_{i=1}^{L-1}\sum_{j=i+1}^{L}\left(z_i - z_j\right)\left(y_i - y_j\right)\right)^2\right] \times \left(\frac{A_0^2\xi^2}{2+\xi^2} + \left(L-1\right)\frac{A_0^2\xi^4}{\left(1+\xi^2\right)^2}\right). \tag{73}$$

Note that the computation for (72) and (73) can be greatly simplified by using the (74) and (75), shown at the top of the page.

$$\mathbb{E}\left[\left(z_i - z_j\right)\left(z_g - z_h\right)\left(y_i - y_j\right)\left(y_g - y_h\right)\right] = \begin{cases} \frac{(2+4r)}{(1+r)^2}\left(2\exp\left(\sigma_z^2\right) - 2\right) & \text{if } i = g \text{ and } j = h \\ 0 & \text{if } i \neq g \text{ and } j \neq h \\ \frac{(1+2r)}{(1+r)^2}\left(\exp\left(\sigma_z^2\right) - 1\right) & \text{if } i = g \text{ and } j \neq h \end{cases} \tag{74}$$

Hence, after some algebra, (73) and (72) are simplified to (38) and (39) respectively.

Appendix D

The definition of Mejer's G-function is expressed as [32]

$$G_{p,q}^{m,n}\left(z\middle|\begin{matrix}a_1,\ldots,a_n,a_{n+1},\ldots,a_p\\ b_1,\ldots,b_m,b_{m+1},\ldots,b_q\end{matrix}\right) = \frac{1}{2\pi i}\int_\Gamma \frac{\prod_{k=1}^{m}\Gamma\left(s+b_k\right)\prod_{k=1}^{n}\Gamma\left(1-a_k-s\right)}{\prod_{k}^{p}\Gamma\left(s+a_k\right)\prod_{t}^{q}\Gamma\left(1-b_k-s\right)}z^{-s}ds, \tag{76}$$

and can be computed by the residual of contour integration [62], i.e.

$$G_{p,q}^{m,n}\left(z\middle|\begin{matrix}a_1,\ldots,a_n,a_{n+1},\ldots,a_p\\ b_1,\ldots,b_m,b_{m+1},\ldots,b_q\end{matrix}\right) = \sum_{k=1}^{n}\sum_{j=0}^{\infty}\mathrm{res}_{s=1-a_k+j} \times \left(\frac{\prod_{k=1}^{m}\Gamma\left(s+b_k\right)\prod_{k=1}^{n}\Gamma\left(1-a_k-s\right)}{\prod_{k=n+1}^{p}\Gamma\left(s+a_k\right)\prod_{k=m+1}^{q}\Gamma\left(1-b_k-s\right)}z^{-s}\right), \tag{77}$$

where no two a_k (for $k = 1, 2, \ldots, n$) differ by an integer, and $p > q$ or $p = q$ with $|z| > 1$. Specifically, the above formula reduces to

$$\lim_{z\to\infty^+} G_{p,q}^{m,n}\left(z\middle|\begin{matrix}a_1,\ldots,a_n,a_{n+1},\ldots,a_p\\ b_1,\ldots,b_m,b_{m+1},\ldots,b_q\end{matrix}\right) = \sum_{k=1}^{n} z^{a_k-1}\frac{\prod_{l=1;l\neq k}^{n}\Gamma\left(a_k-a_l\right)\prod_{l=1}^{m}\Gamma\left(1+b_l-a_k\right)}{\prod_{l=n+1}^{p}\Gamma\left(1+a_l-a_k\right)\prod_{l=m+1}^{q}\Gamma\left(a_k-b_l\right)} = z^{a_k^*-1}\frac{\prod_{l=1;l\neq k}^{n}\Gamma\left(a_k^*-a_l\right)\prod_{l=1}^{m}\Gamma\left(1+b_l-a_k^*\right)}{\prod_{l=n+1}^{p}\Gamma\left(1+a_l-a_k^*\right)\prod_{l=m+1}^{q}\Gamma\left(a_k^*-b_l\right)}, \tag{78}$$

where in (78), $a_k^* = \max\{a_k\}_{k=1}^n$, the second equality holds due to [12, eqn. (41)], and the last equality holds when $a_k - 1 < 0$ for $k = 1, 2, \ldots, n$.

References

[1] M. Z. Chowdhury, M. T. Hossan, A. Islam, and Y. M. Jang, "A comparative survey of optical wireless technologies: Architectures and applications," *IEEE Access*, vol. 6, pp. 9819–9840, 2018.

[2] C. H. de Souza Lopes *et al.*, "Non-standalone 5G NR fiber-wireless system using fso and fiber-optics fronthauls," *J. Lightw. Technol.*, vol. 39, no. 2, pp. 406–417, Jan. 2021. [Online]. Available: http://opg.optica.org/jlt/abstract.cfm?URI=jlt- 39--2-406

[3] W. Gappmair, "Further results on the capacity of free-space optical channels in turbulent atmosphere," *IET Commun.*, vol. 5, pp. 1262–1267, Jun. 2011.

[4] X. Zhu and J. Kahn, "Free-space optical communication through atmospheric turbulence channels," *IEEE Trans. Commun.*, vol. 50, no. 8, pp. 1293–1300, Aug. 2002.

[5] Z. Wang, W.-D. Zhong, C. Yu, and S. Fu, "Performance improvement of on-off-keying free-space optical transmission systems by a co-propagating reference continuous wave light," *Opt. Exp.*, vol. 20, no. 8, pp. 9284–9295, Apr. 2012.

[6] A. L. C., *Laser Beam Propagation Through Random Media/L. C. Andrews and R. L. Phillips*, 2nd ed. Bellingham, Wash: SPIE Press, 2005.

[7] F. S. Vetelino, C. Young, L. Andrews, and J. Recolons, "Aperture averaging effects on the probability density of irradiance fluctuations in moderate-to-strong turbulence," *Appl. Opt.*, vol. 46, no. 11, pp. 2099–2108, Apr. 2007.

[8] J. H. Churnside and S. F. Clifford, "Log-normal rician probability-density function of optical scintillations in the turbulent atmosphere," *J. Opt. Soc. Am A*, vol. 4, no. 10, pp. 1923–1930, Oct. 1987.

[9] M. A. Al-Habash, L. C. Andrews, and R. L. Phillips, "Mathematical model for the irradiance probability density function of a laser beam propagating through turbulent media," *Opt. Eng.*, vol. 40, no. 8, pp. 1554–1562, 2001.

[10] A. Jurado-Navas, J. María Garrido-Balsells, J. Francisco Paris, and A. Puerta-Notario, "A unifying statistical model for atmospheric optical scintillation," in *Numerical Simulations Physical Engineering Processes*. Rijeka, Croatia: InTech, Sep. 2011, pp. 181–206.

[11] N. Wang and J. Cheng, "Moment-based estimation for the shape parameters of the gamma-gamma atmospheric turbulence model," *Opt. Exp.*, vol. 18, no. 12, pp. 12824–12831, Jun. 2010.

[12] I. S. Ansari, F. Yilmaz, and M.-S. Alouini, "Performance analysis of free-space optical links over Málaga turbulence channels with pointing errors," *IEEE Trans. Wireless Commun.*, vol. 15, no. 1, pp. 91–102, Jan. 2016.

[13] D. K. Borah and D. G. Voelz, "Pointing error effects on free-space optical communication links in the presence of atmospheric turbulence," *J. Lightw. Technol.*, vol. 27, no. 18, pp. 3965–3973, 2009.

[14] A. A. Farid and S. Hranilovic, "Outage capacity optimization for free-space optical links with pointing errors," *J. Lightw. Technol.*, vol. 25, no. 7, pp. 1702–1710, 2007.

[15] R. Boluda-Ruiz, A. García-Zambrana, B. Castillo-Vázquez, and C. Castillo-Vázquez, "On the capacity of MISO FSO systems over gamma-gamma and misalignment fading channels," *Opt. Exp.*, vol. 23, no. 17, pp. 22371–22385, Aug. 2015.

[16] M. R. Bhatnagar and Z. Ghassemlooy, "Performance analysis of gamma-gamma fading FSO MIMO links with pointing errors," *J. Lightw. Technol.*, vol. 34, no. 9, pp. 2158–2169, 2016.

[17] M. Miao and X. Li, "Novel approximate distribution of the sum of gamma-gamma variates with pointing errors and applications in MIMO FSO links," *Opt. Commun.*, vol. 486, 2021, Art. no. 126780.

[18] J. Ding, S. Yu, Y. Fu, J. Ma, and L. Tan, "New approximate and asymptotic closed-form expressions for the outage probability and the average BER of MIMO-FSO system with MRC diversity technique over gamma-gamma fading channels with generalized pointing errors," *Opt. Commun.*, vol. 456, 2020, Art. no. 124633.

[19] E. Illi, F. El Bouanani, and F. Ayoub, "On the distribution of the sum of Málaga-$\mathcal{M}$ random variables and applications," *IEEE Trans. Veh. Technol.*, vol. 69, no. 11, pp. 13996–14000, Nov. 2020.

[20] M. J. Saber and S. M. S. Sadough, "On secure free-space optical communications over Málaga turbulence channels," *IEEE Wireless Commun. Lett.*, vol. 6, no. 2, pp. 274–277, Apr. 2017.

[21] F. Yang and J. Cheng, "Coherent free-space optical communications in lognormal-rician turbulence," *IEEE Commun. Lett.*, vol. 16, no. 11, pp. 1872–1875, Nov. 2012.

[22] M. Miao and X. Li, "Error performance analysis of optical communication over lognormal-rician turbulence channel using Gram-Charlier series," *J. Opt. Commun.*, vol. 2021, 2021, Art. no. 000010151520200241.

[23] F. Yilmaz and M.-S. Alouini, "Novel asymptotic results on the high-order statistics of the channel capacity over generalized fading channels," in *Proc. IEEE 13th Int. Workshop Signal Process. Adv. Wireless Commun.*, 2012, pp. 389–393.

[24] I. S. Ansari, M.-S. Alouini, and J. Cheng, "On the capacity of FSO links under lognormal and rician-lognormal turbulences," in *Proc. IEEE 80th Veh. Technol. Conf.*, 2014, pp. 1–6.

[25] M. Miao and X. Li, "Performance analysis of FSO systems over a lognormal-rician turbulence channel with generalized pointing errors," *J. Lightw. Technol.*, to be published, doi: 10.1109/JLT.2022.3161940.

[26] S. M. Navidpour, M. Uysal, and M. Kavehrad, "BER performance of free-space optical transmission with spatial diversity," *IEEE Trans. Wireless Commun.*, vol. 6, no. 8, pp. 2813–2819, Aug. 2007.

[27] P. Deng, M. Kavehrad, Z. Liu, Z. Zhou, and X. Yuan, "Capacity of MIMO free space optical communications using multiple partially coherent beams propagation through non-kolmogorov strong turbulence," *Opt. Exp.*, vol. 21, no. 13, pp. 15213–15229, Jul. 2013.

[28] E. Lee and V. Chan, "Part 1: Optical communication over the clear turbulent atmospheric channel using diversity," *IEEE J. Sel. Areas Commun.*, vol. 22, no. 9, pp. 1896–1906, Nov. 2004.

[29] J. Zhang, L. Dai, Y. Han, Y. Zhang, and Z. Wang, "On the ergodic capacity of MIMO free-space optical systems over turbulence channels," *IEEE J. Sel. Areas Commun.*, vol. 33, no. 9, pp. 1925–1934, Sep. 2015.

[30] V. P. Thanh, C.-T. Truong, and T. P. Anh, "On the MGF-based approximation of the sum of independent gamma-gamma random variables," in *Proc. IEEE 81st Veh. Technol. Conf.*, 2015, pp. 1–5.

[31] C. Chayawan and V. Aalo, "On the outage probability of optimum combining and maximal ratio combining schemes in an interference-limited rice fading channel," *IEEE Trans. Commun.*, vol. 50, no. 4, pp. 532–535, Apr. 2002.

[32] I. S. Gradshteyn and I. M. Ryzhik, *Table of Integrals, Series, and Products*, 7th ed. Burlington, MA, USA: Academic Press, 2007.

[33] X. Liu, "Free-space optics optimization models for building sway and atmospheric interference using variable wavelength," *IEEE Trans. Commun.*, vol. 57, no. 2, pp. 492–498, Feb. 2009.

[34] E. Farooq, A. Sahu, and S. K. Gupta, "Survey on FSO communication system–limitations and enhancement techniques," in *Optical and Wireless Technologies*, V. Janyani, M. Tiwari, G. Singh, and P. Minzioni, Eds. Singapore: Springer, 2018, pp. 255–264.

[35] N. D. Chatzidiamantis and G. K. Karagiannidis, "On the distribution of the sum of gamma-gamma variates and applications in RF and optical wireless communications," *IEEE Tran. Commun.*, vol. 59, no. 5, pp. 1298–1308, May 2011.

[36] L. Fenton, "The sum of log-normal probability distributions in scatter transmission systems," *IRE Trans. Commun. Syst.*, vol. 8, no. 1, pp. 57–67, 1960.

[37] F. Yilmaz and M.-S. Alouini, "A novel unified expression for the capacity and bit error probability of wireless communication systems over generalized fading channels," *IEEE Trans. Commun.*, vol. 60, no. 7, pp. 1862–1876, Jul. 2012.

[38] C. Fox, "The G and H functions as symmetrical Fourier kernels," *Trans. Amer. Math. Soc.*, vol. 98, no. 3, pp. 395–429, 1961.

[39] A. Soulimani, M. Benjillali, H. Chergui, and D. B. da Costa, "Multihop weibull-fading communications: Performance analysis framework and applications," *J. Franklin Inst.*, vol. 358, no. 15, pp. 8012–8044, 2021.

[40] K. P. Peppas, F. Lazarakis, A. Alexandridis, and K. Dangakis, "Simple, accurate formula for the average bit error probability of multiple-input multiple-output free-space optical links over negative exponential turbulence channels," *Opt. Lett.*, vol. 37, no. 15, pp. 3243–3245, Aug. 2012.

[41] M. Abramowitz and I. A. Stegun, Eds., *Handbook of Mathematical Functions with Formulas, Graphs, and Mathematical Tables*, 10th ed. Washington, DC, USA: U. S, Government printing office, 1972.

[42] J. Wu, N. Mehta, and J. Zhang, "Flexible lognormal sum approximation method," in *Proc. IEEE Glob. Telecommun. Conf.*, 2005, vol. 6, pp. 3413–3417.

[43] G. H. Golub and J. H. Welsch, "Calculation of gauss quadrature rules," *Math. Comp.*, vol. 23, no. 106, pp. 221–230, 1969.

[44] M. D. Renzo, F. Graziosi, and F. Santucci, "A comprehensive framework for performance analysis of cooperative multi-hop wireless systems over log-normal fading channels," *IEEE Trans. Commun.*, vol. 58, no. 2, pp. 531–544, 2010.

[45] H. Moradi, M. Falahpour, H. H. Refai, P. G. LoPresti, and M. Atiquzzaman, "BER analysis of optical wireless signals through lognormal fading channels with perfect CSI," in *Proc. 17th Int. Conf. Telecommun.*, 2010, pp. 493–497.

[46] B. Kumbhani and R. S. Kshetrimayum, *MIMO Wireless Communications Over Generalized Fading Channels*, 1st ed. USA: CRC Press, Inc., 2017.

[47] M. Yacoub, "The $\kappa - \mu$ distribution and the $\eta - \mu$ distribution," *IEEE Antennas Propag. Mag.*, vol. 49, no. 1, pp. 68–81, Feb. 2007.

[48] B. D. Carter and M. D. Springer, "The distribution of products, quotients and powers of independent h-function variates," *SIAM J. Appl. Math.*, vol. 33, no. 4, pp. 542–558, 1977.

[49] A. M. Mathai, *The H-Function Theory and Applications*. New York,USA: Springer, 2009.

[50] V. S. Adamchik and O. I. Marichev, "The algorithm for calculating integrals of hypergeometric type functions and its realization in reduce system," in *Proc. Int. Symp. Symbolic Algebr. Comput.*, New York, NY, USA: Association for Computing Machinery, 1990, pp. 212–224.

[51] A. Papoulis and S. U. Pillai, *Probability, Random Variables, and Stochastic Processes*, 4th ed. Boston, USA: McGraw Hill, 2002.

[52] Wolfram Research, Inc., "The Wolfram functions site." [Online]. Available: https://functions.wolfram.com/HypergeometricFunctions/MeijerG/21/02/03/01/0002/

[53] D. Tse and P. Viswanath, *MIMO II: Capacity and Multiplexing Architectures*. Cambridge, U.K.: Cambridge Univ. Press, 2005, pp. 332–376.

[54] R. Boluda-Ruiz, A. García-Zambrana, B. Castillo-Vázquez, C. Castillo-Vázquez, and K. Qaraqe, "On the beam width optimization for the ergodic capacity of FSO channels with misalignment errors modeled by beckmann distributions," *IEEE Photon. J.*, vol. 10, no. 5, Oct. 2018, Art no. 7907414.

[55] R. Boluda-Ruiz, A. García-Zambrana, B. Castillo-Vázquez, and C. Castillo-Vázquez, "Impact of nonzero boresight pointing error on ergodic capacity of MIMO FSO communication systems," *Opt. Exp.*, vol. 24, no. 4, pp. 3513–3534, Feb. 2016.

[56] Wolfram Research, Inc., "The Wolfram functions site." [Online]. Available: https://functions.wolfram.com/HypergeometricFunctions/MeijerG/03/01/03/12/0004

[57] E. Bayaki, R. Schober, and R. K. Mallik, "Performance analysis of MIMO free-space optical systems in gamma-gamma fading," *IEEE Trans. Commun.*, vol. 57, no. 11, pp. 3415–3424, Nov. 2009.

[58] A. P. Prudnikov, Y. A. Brychkov, and O. I. Marichev, *Integrals and Series of Special Functions*. New York, NY, USA: Gordon and Breach, (in Russian), 1983.

[59] L. Yang, J. Cheng, and J. F. Holzman, "Maximum likelihood estimation of the lognormal-rician FSO channel model," *IEEE Photon. Technol. Lett.*, vol. 27, no. 15, pp. 1656–1659, Aug. 2015.

[60] S. Panic, M. Stefanovic, J. Anastasov, and P. Spalevic, *Fading and Interference Mitigation in Wireless Communications*, 1st ed. USA: Boca Raton, FL, USA: CRC Press, Inc., 2013.

[61] R. Singh and M. Rawat, "Performance analysis of physical layer security over weibull/lognormal composite fading channel with MRC reception," *AEU - Int. J. Electron. Commun*, vol. 110, 2019, Art. no. 152849.

[62] Wolfram Research, Inc., "The Wolfram functions site." [Online]. Available: https://functions.wolfram.com/HypergeometricFunctions/MeijerG/06/06/0002